Electronic Supplementary Material (ESI) for Journal of Materials Chemistry A.

Supporting Information

pH-dependent Hydrogen Evolution by Spatially Confined Ruthenium on Hollow N-doped Carbon Nanocages as Mott-Schottky Catalyst

Bidushi Sarkar[‡a], Debanjan Das[‡a] and Karuna Kar Nanda*[a]

[a]Materials Research Centre, Indian Institute of Science, Bangalore-560012, India

*E-mail: nanda@iisc.ac.in

MATERIALS AND METHODS

Chemicals

Zinc nitrate hexahydrate ($Zn(NO_3)_2 \bullet 6H_2O$), 2- methyl imidazole ($CH_3C_3H_2N_2H$), methanol and ruthenium acetylacetonate ($(C_5H_7O_2)_3Ru$) were procured from Sigma-Aldrich and carbon black Vulcan XC-72. Millipore water obtained from a Merck Milli-Q system was used for the experiments.

Material synthesis

Synthesis of ZIF-8: At room temperature, 1.46 g of zinc nitrate hexahydrate and 3.25 g of 2-methyl imidazole was dissolved in 50 mL of methanol separately. The 2- methyl imidazole solution was then added slowly into the zinc solution with continuous magnetic stirring for 15 min and was left undisturbed overnight to obtain a white solid. The solid was collected by centrifugation (5000 rpm), washed with methanol several times, and dried at 80 °C to get the ZIF-8 crystals.

Synthesis of NC: As synthesized, ZIF-8 (100 mg) was added in a close quartz tube and pyrolyzed at 900 °C for two h under N_2 atmosphere in a Lenton tube furnace to form NC as the final product.

Synthesis of Ru@NCN: As synthesized ZIF-8, and ruthenium acetylacetonate $Ru(acac)_3$ were taken (weight ratio 3:1, respectively) and ground in mortar-pestle. The obtained powder was added into a one-end closed quartz tube and put to pyrolysis at 900 °C for two h under N_2 atmosphere in a Lenton tube furnace. The resulted black product was named Ru@NCN. The catalyst with this precursor ratio is mentioned as Ru@NCN in the manuscript, unless specified.

Same procedure was followed with a different ZIF-8 to $Ru(acac)_3$ ratio as 2:1, and 5:1 to obtain Ru@NCN1 and Ru@NCN2, respectively.

Synthesis of Ru@CB: Commercial carbon black Vulcan XC-72 and ruthenium acetylacetonate were taken (weight ratio 3:1, respectively), ground well in mortar-pestle, and subjected to pyrolysis at 900 °C for 2 h under N_2 atmosphere. The as-obtained product was named Ru@CB.

Synthesis of Ru@Pt and Ru@Cu: Metallic Ru (0.3 mg/cm^2 loading) is drop casted on a Pt working electrode (diameter, 2mm) to obtain Ru@Pt. Similarly, metallic Ru is electrodeposited on Cu foil in an area of 1 cm*1 cm to obtain Ru@Cu.

Material Characterizations

X-ray diffraction (XRD) data of as-prepared samples were collected at room temperature with a 2θ scan range of 10−90° using an X-ray diffractometer, PANalytical equipped with Cu Kα radiation (1.54 Å). The XRD of samples after the HER studies were collected using Bruker D8 Advance. Raman spectra of the samples were recorded on a WITec system (excitation wavelength = 532 nm). Thermogravimetric analysis (TGA) was done on TGA TA instruments (Q50 series) in nitrogen atmosphere. The specific Brunauer- Emmett-Teller (BET) surface area was evaluated using an Autosorb iQ, Quantachrome Instruments. The scanning electron microscopy (SEM) images were obtained using Karl Ziess Ultra 55 FE-SEM. The transmission electron microscopy (TEM) images, high-resolution TEM (HRTEM), high-angle annular dark-field imaging - scanning transmission electron microscopy (HAADF - STEM) and elemental mapping were carried out using FEI Titan Themis 300 at an accelerating voltage of 300 kV. X-ray photoelectron spectroscopy (XPS) was performed on Thermo Scientific ESCALAB 250 with a monochromatic Al K_α source (1486.6 eV). The calibration of all elements' binding energy was done by placing the C 1s peak at 284.6 eV. The inductively coupled plasma mass spectrophotometry (ICPMS) was done on a quadrupole ICPMS Thermo X Series II.

Electrochemical measurements

All the electrochemical measurements were carried out using a conventional three-electrode cell on a CHI 750E workstation. The commercial glassy carbon electrode (GCE, 0.07 cm^2), saturated calomel electrode (SCE), and graphite rod as the working, reference, and counter electrode, respectively. To prepare the working electrode, 2 mg of catalyst was taken, added 200 µL of ethanol, and 50 µL of water followed by 20 µL of a 5 wt % Nafion 117 solution. The as-prepared ink was sonicated for 30 min and 2.5 µL of the ink was drop-casted onto the GCE and air-dried (loading ~ 0.26 mg cm^{-2}). For comparison of activity, the commercial 20 wt % Pt/C purchased from Johnson Matthey Co., HiSPEC™ 3000 was used. The potentials measured were converted to potential versus reversible hydrogen electrode (RHE) using the equation: $E\ (_{vs\ RHE}) = E\ (_{vs\ SCE}) + E_{SCE^\circ} + 0.059$ pH. The measurements were carried out in 1 M KOH, 1 M H_2SO_4 and 1 M phosphate buffer saline (PBS) solution, respectively after purging with N_2 gas for 30 min.

Electrochemical active surface area (ECSA) is evaluated using the double layer capacitance (C_{dl}) using the following equation,

$$ECSA = C_{dl}/C_s$$

where Cs is the specific capacitance that is 0.04 and 0.035 mF/cm^2 in alkaline and acidic media, respectively.

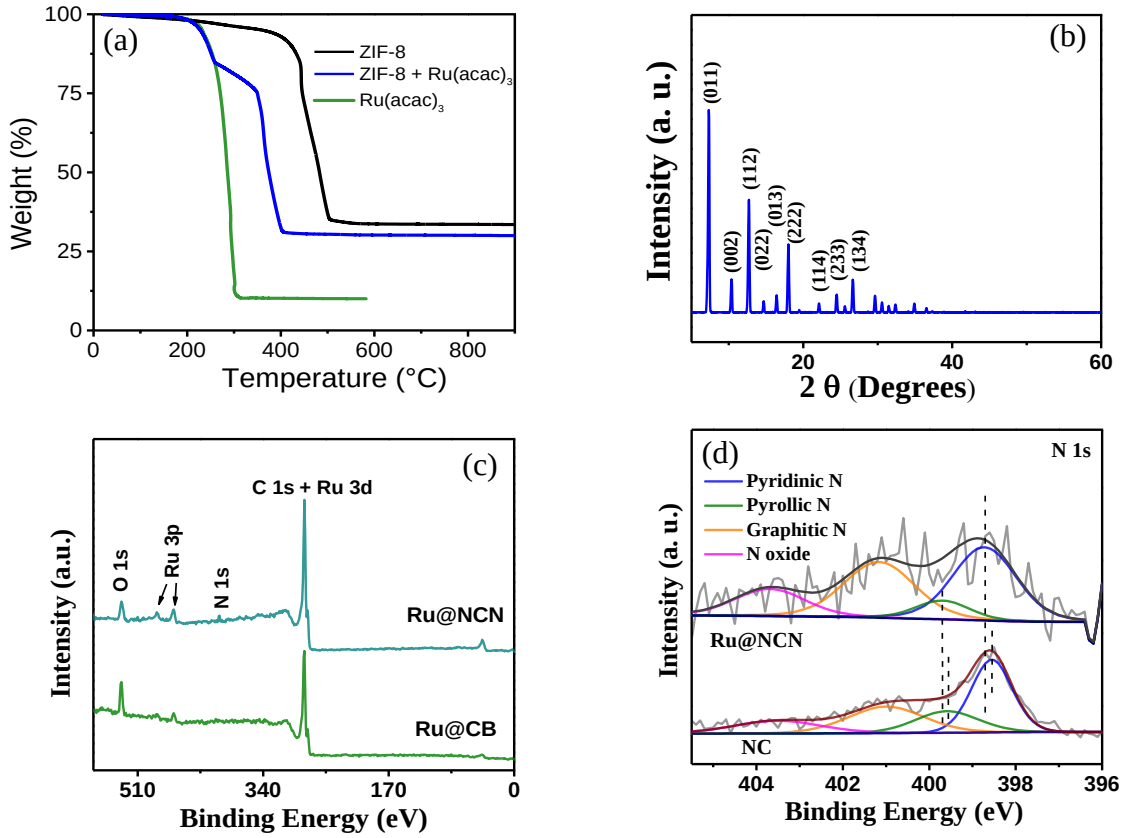

Figure S1. (a) TGA in N_2 atmosphere of ZIF-8, $Ru(acac)_3$ and the precursor mixture (ZIF-8 + $Ru(acac)_3$) to obtain Ru@NCN, (b) XRD pattern of ZIF-8. (c) Survey XPS spectra of Ru@NCN and Ru@CB, and (d) HRXPS N 1s spectra of Ru@NCN and NC.

The TGA of the precursors (ZIF-8 and $Ru(acac)_3$) is shown in Figure S1(a). The decomposition of $Ru(acac)_3$ to RuO_2 is marked by a steep fall at 175-300 °C with subsequent release of volatiles (CO, CO_2 and H_2O) due to decomposition of acetylacetonate ligand.[1, 2] The TGA of ZIF-8 precursor displays a weight loss of ~ 4 % up to 300 °C that can be attributed to loss of H_2O and removal of guest molecules (unreacted imidazole ligand) adsorbed and trapped within ZIF-8. Further loss up to 390 °C is due to partial dissociation of the methyl groups. A rapid fall in the range 390-510 °C indicates the carbonization of ZIF-8 with removal of volatile CO_x and NO_x.[3] Now, when both the precursors are subjected to physical mixing (ZIF-8 + $Ru(acac)_3$), a three-step dissociation is observed in the TGA. A weight loss of 16 % at ~ 260 °C occurs because of decomposition of $Ru(acac)_3$ followed by partial dissociation of methyl groups till 350 °C. A total weight loss of 69 % is observed at 405 °C that marks the carbonization of the precursor.

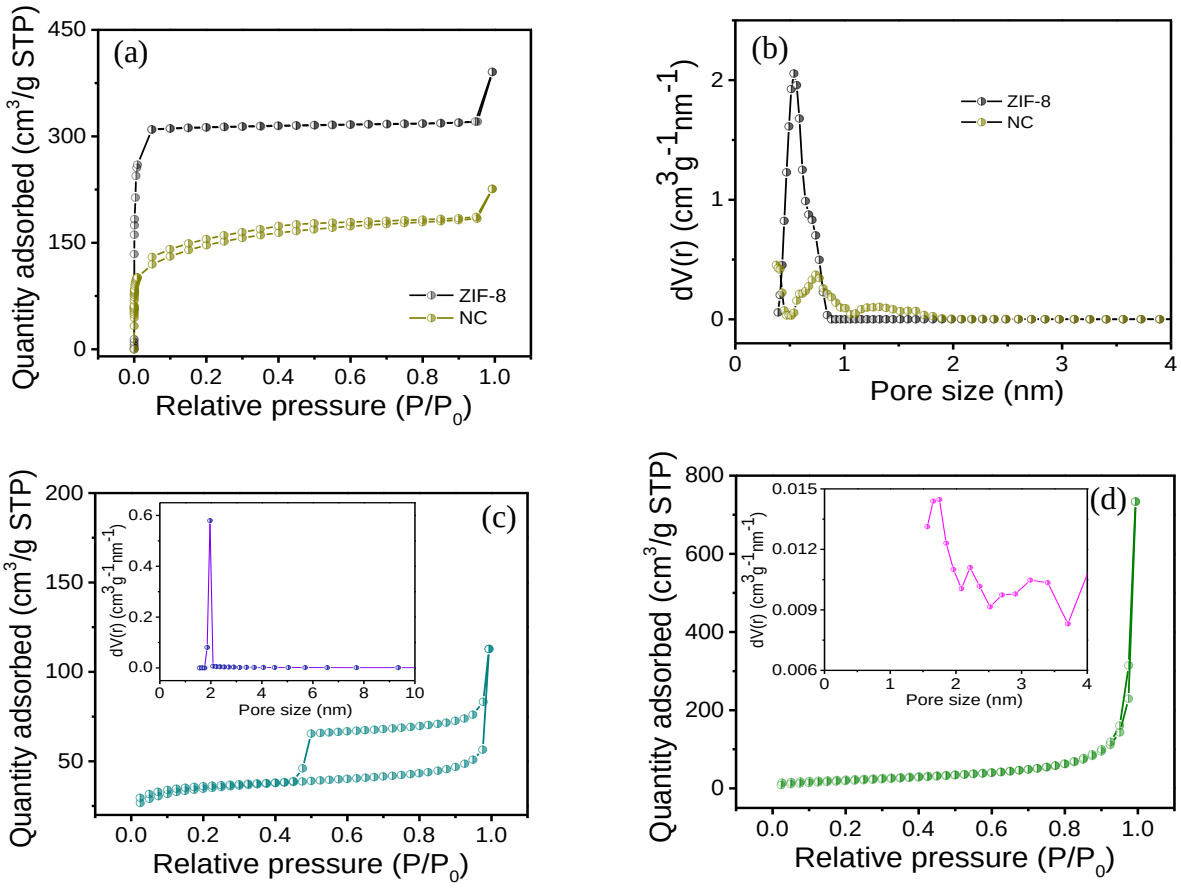

Figure S2 N_2 adsorption/desorption isotherms for BET surface area and BJH plot for pore radius of (a, b) ZIF-8 and NC, (c) Ru@NCN and (d) Ru@CB.

Table S1. Specific surface area, average pore size and volume using BET-BJH method for different samples.

	Specific surface area (m^2/g)	Average pore size (radius, nm)	Pore volume (cc/g)
ZIF-8	1304.29	0.53	0.46
NC	520.57	0.37	0.28
Ru@NCN	127.87	1.96	0.15
Ru@CB	82.48	1.75	1.14

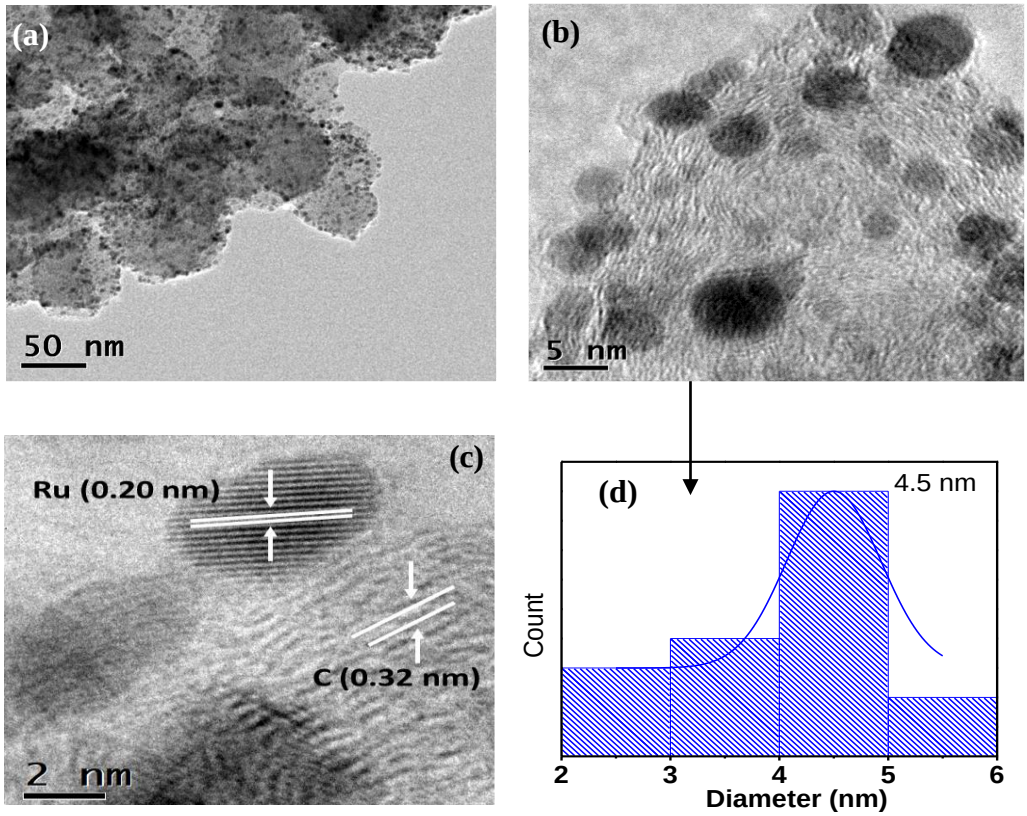

Figure S3 (a, b) TEM image, (c) HRTEM image and (d) size distribution curve of Ru@CB.

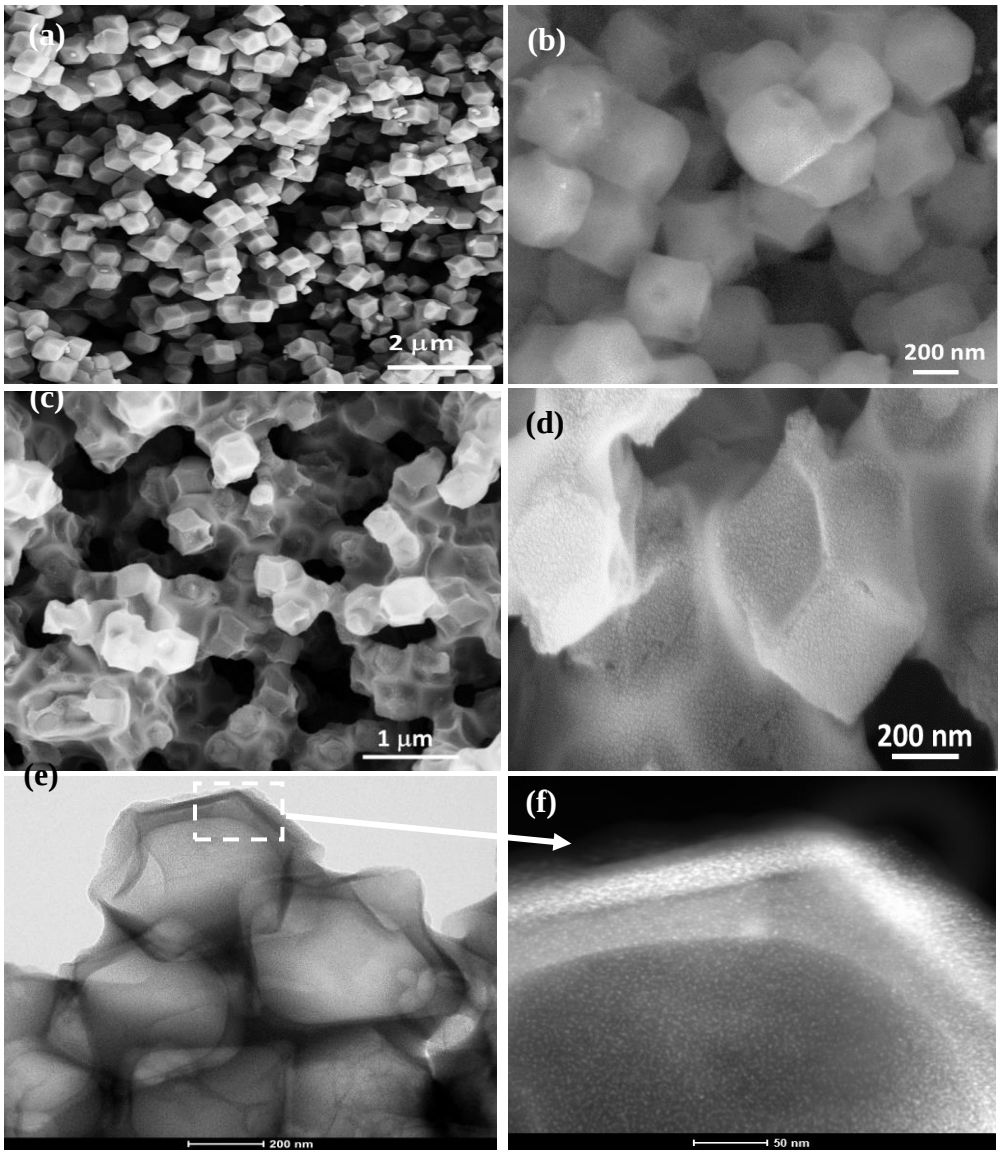

Figure S4. SEM image of (a) ZIF-8, (b) NC, (c, d) Ru@NCN, and (e) TEM image and (f) HAADF-STEM image of Ru@NCN.

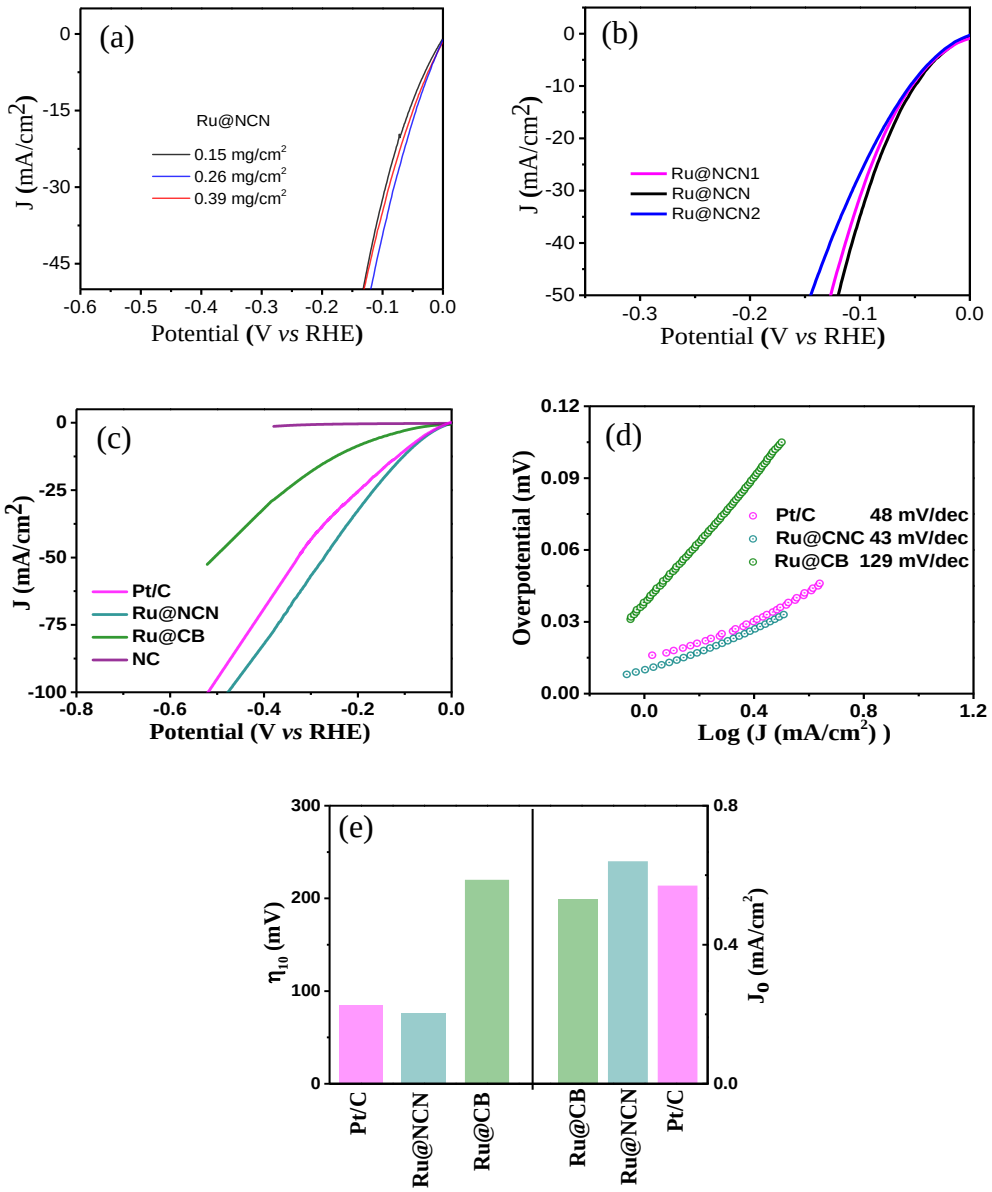

Figure S5. (a) Variation of HER activity with catalyst loading in 1 M KOH solution for Ru@NCN. The optimized loading is 0.26 mg/cm^2. (b) LSV polarization curves of Ru@NCN with different precursor ratio for HER in 0.5 M H_2SO_4. (c) Comparison of HER polarization curve of as-synthesized samples with commercial 20 wt % Pt/C at a scan rate of 5 mV/s. (d) Tafel slope and (e) Bar graph depicting the overpotential required to reach the current density of 10 mA/cm^2 (left) and exchange current density, J_o (mA/cm^2) for the samples (right) in 1 M PBS.

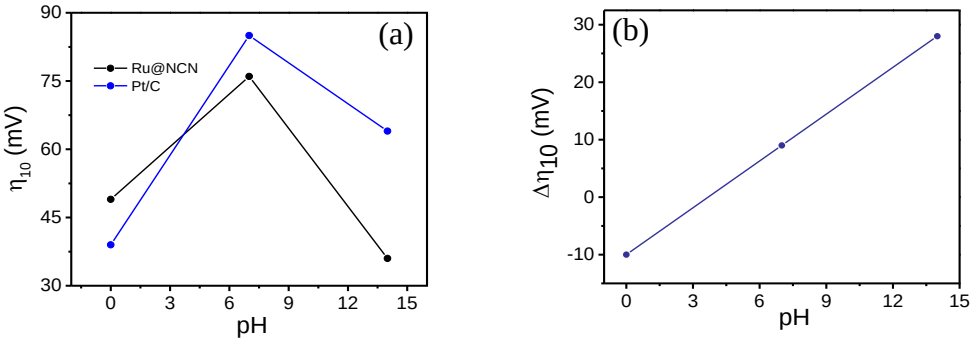

Figure S6 (a) Variation of h_{10} (overpotential required to reach a current density of 10 mA/cm^2) for Ru@NCN and Pt/C with changing pH. (b) Plot of Dh_{10} ($h_{Pt/C}$ - $h_{Ru@NCN}$) with change in pH.

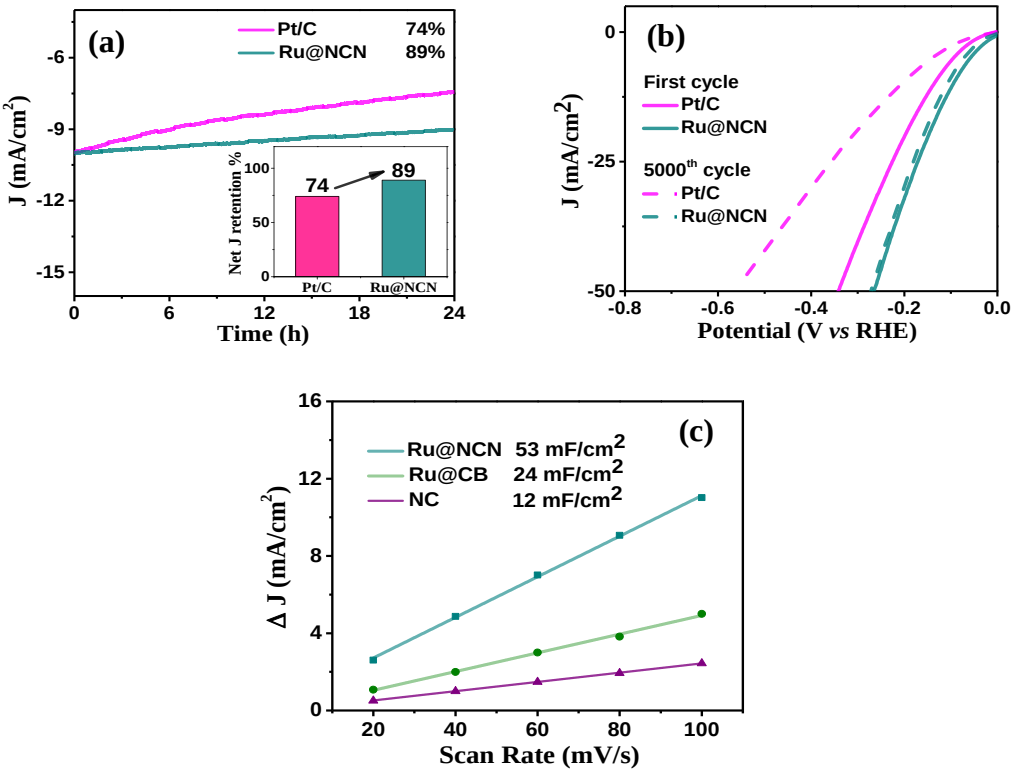

Figure S7. (a) Chronoamperometric studies done for a time duration of 24 h. inset- bar graph depicts the increase in the net current retention % from commercial Pt/C to as-synthesized Ru@NCN. (b) LSV curve after the first and 5000th cycle of the ADT at a scan rate of 100 mV/s for Pt/C and Ru@NCN. and (c) C_{dl} calculated from the CV curves studied in the non-faradaic region for the samples in 1 M PBS.

Table S2. Comparison of HER activity of as-synthesized catalyst with previously reported Ru-based catalysts in alkaline, acidic, and neutral media.

Catalyst	**Loading (mg/cm^2)**	**Medium**	**E@10 mA/cm^2 (mV)**	**Tafel slope (mV/dec)**	**Reference**
Ru@NCN	***0.26***	***1 M KOH***	***36***	***33***	***This work***
Ru-MoS2/CC	12.4	1 M KOH	41	114	*4*
Ru-NGC	-		40	65	*5*
$Ru/C_3N_4/C$	0.204	1 M KOH	79	-	*6*
RuP_2@NPC	1.00	1 M KOH	52	69	7
Ultrafine Ru/NG tube	0.428	1 M KOH	45	81	8
RuCo@NC	0.275	1 M KOH	28	31	9
Ultrafine Ru/N-G	-	1 M KOH	40	76	10
Ru@CN	-	1 M KOH	32	53	11
Pd-Ru@NG	-	1 M KOH	42	73	12
Ru/NC	-		21	~ 31	13
Ru@NCN	***0.26***	***0.5 M H_2SO_4***	***49***	***41***	***This work***
Pd@Ru NRs	-	0.5 M H_2SO_4	37	33	14
Ru-HPC	0.2	0.5 M H_2SO_4	61.6	66.8	15
0.27-RuO_2@C	-	0.5 M H_2SO_4	33	53	*16*
s-RuS_2/S-rGO	-	0.5 M H_2SO_4	69	64	*17*
Ru_xFe_ySez	0.8	0.5 M H_2SO_4	85	111	18

Ru_xP	-	0.5 M H_2SO_4	62	129	[19]
Ru-based nanoparticles	0.12	0.5 M H_2SO_4	65	100	[20]
$Ni_{43}Ru_{57}$	0.28	0.5 M H_2SO_4	41	~31	[21]
Ru@NCN	***0.26***	***1 M PBS***	***76***	***43***	***This work***
Ru@Co–SAs/N–C	-	1 M PBS	55	82	[22]
RuP_2@NPC	1	1 M PBS	57	87	[7]
Ru@CN-0.16	0.048	1 M PBS	100	-	[11]
Ru/MeOH/THF	0.352	0.1 M PBS	83	80	[23]
1D-RuO_2-CNx	0.17	0.1 M PBS	356	135	[24]

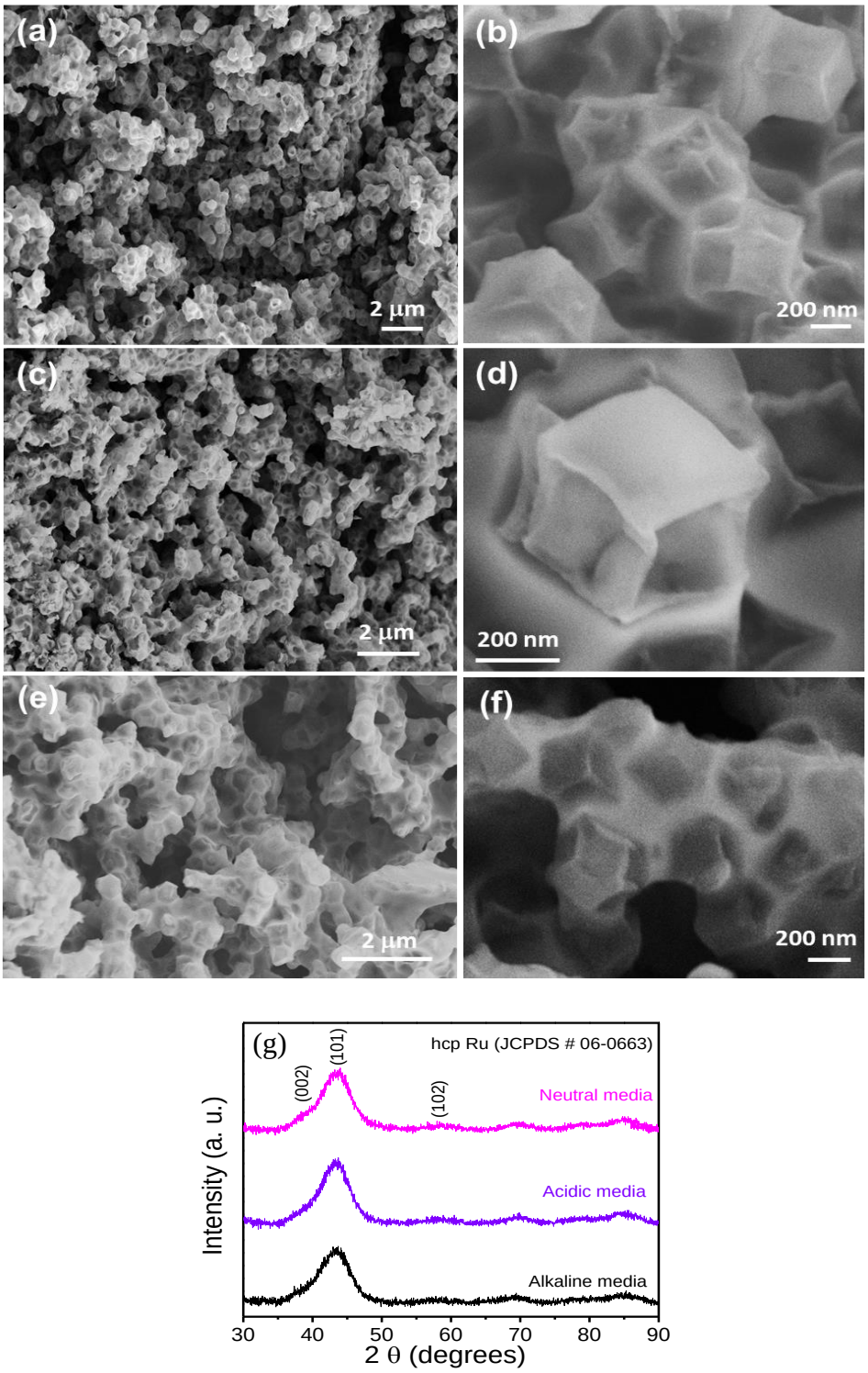

Figure S8. SEM images of Ru@NCN after stability test in (a, b) alkaline, (c, d) acidic, and (e, f) neutral media, (g) XRD pattern of Ru@NCN after stability testing in respective media.

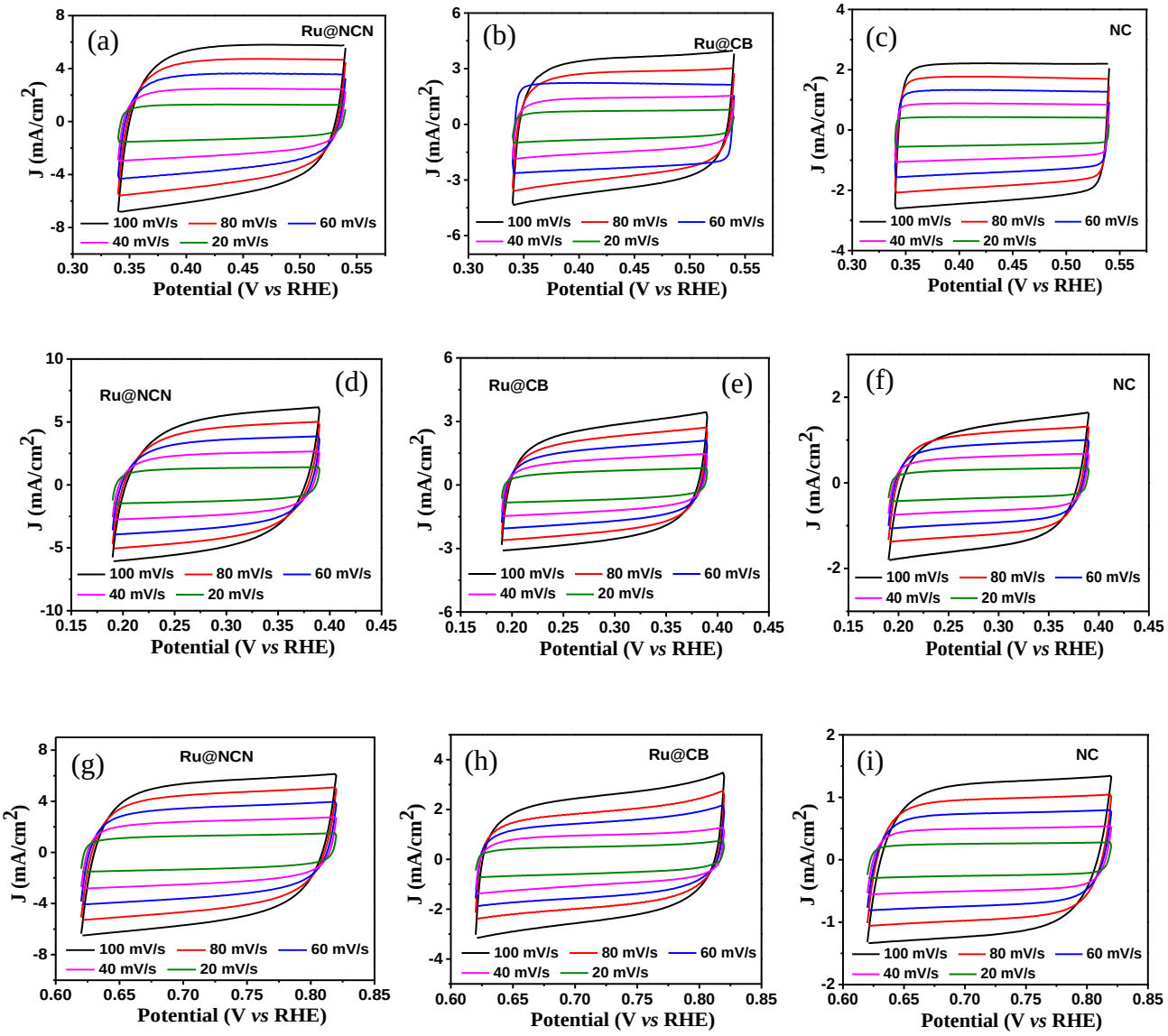

Figure S9. CV in the non-faradaic region at different scan rates (20 to 100 mV/s) to calculate the C_{dl} in (a-c) alkaline, (d-f) acidic, and (g-i) neutral media for Ru@NCN, Ru@CB and NC, respectively.

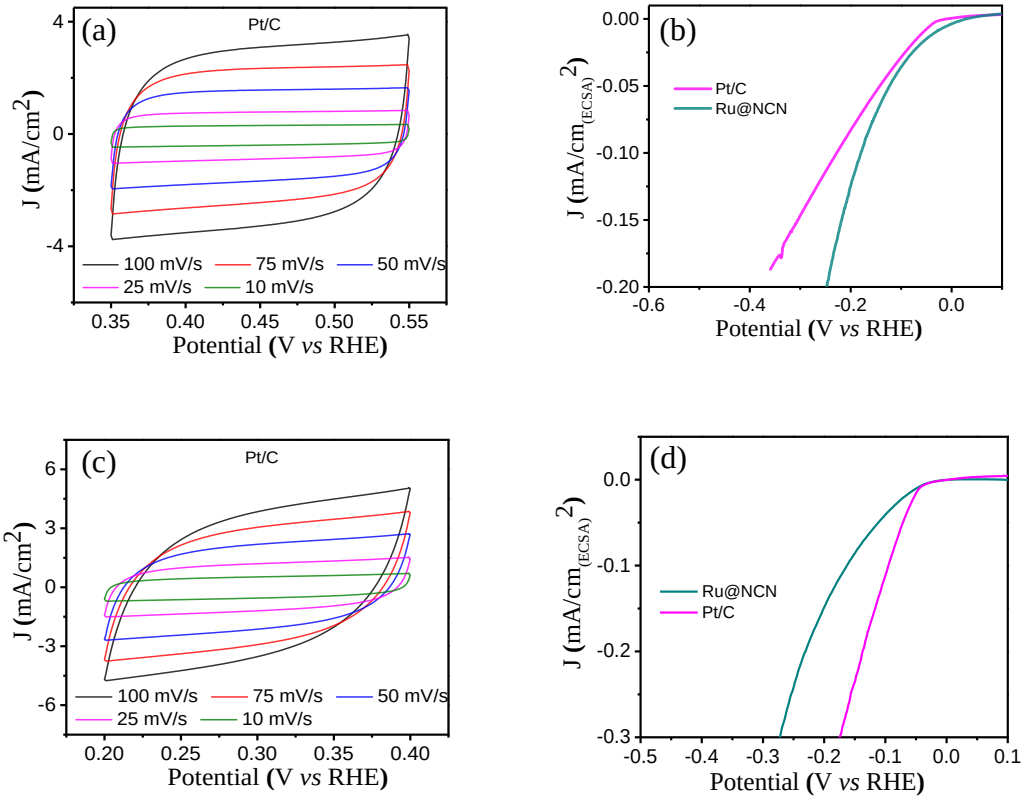

Figure S10. CV in the non-faradaic region at different scan rates (10 to 100 mV/s) to calculate the C_{dl} in (a) alkaline, (c) acidic media, ECSA normalized LSV polarization curve in (b) alkaline and (d) acidic media.

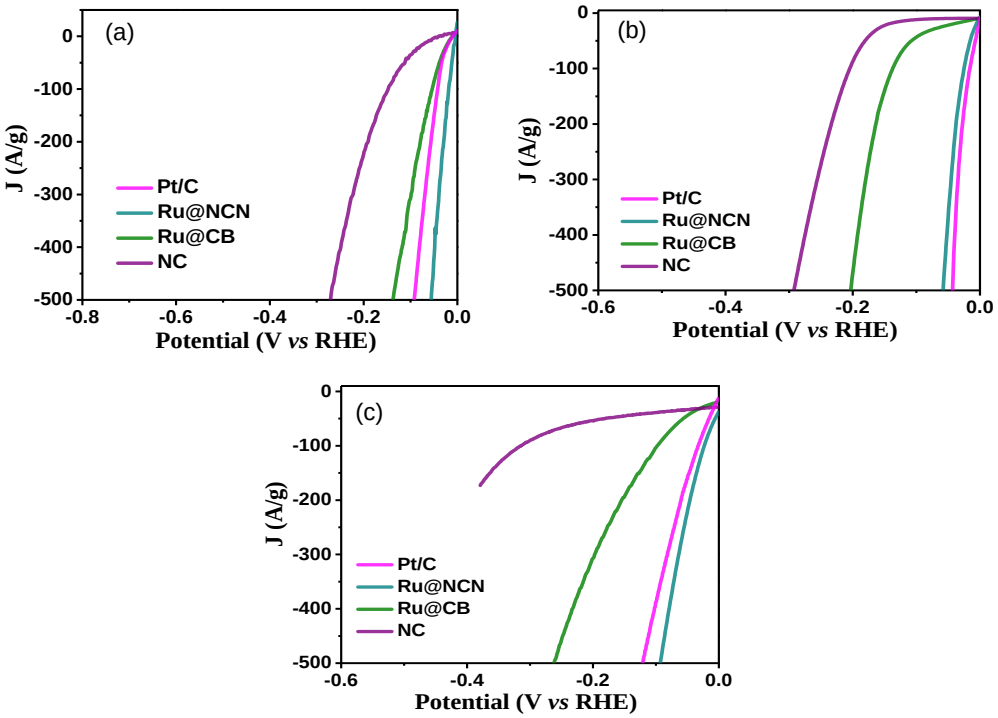

Figure S11. Mass normalized LSV in (a) alkaline, (b) acidic, and (c) neutral media.

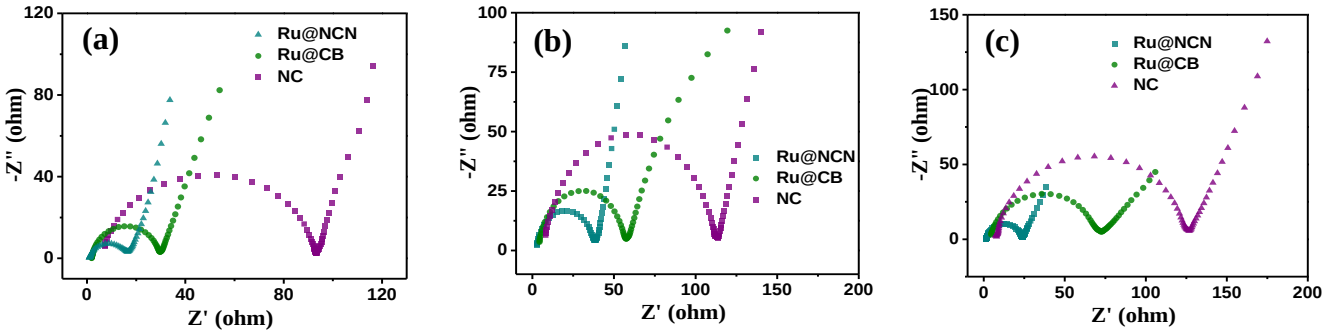

Figure S12. Nyquist plot for Ru@NCN, Ru@CB and NC in (a) alkaline (b) acidic and (c) neutral media.

Table S3 Charge transfer (R_{ct}) and solution (R_s) resistance obtained from the Nyquist plots for the various catalysts in the universal pH range.

	$R_{ct} + R_s$		
	Alkaline media	**Acidic media**	**Neutral media**
Ru@NCN	17.3	38.7	24.3
Ru@CB	29.4	58.1	73.9
NC	92.9	113.0	128.2

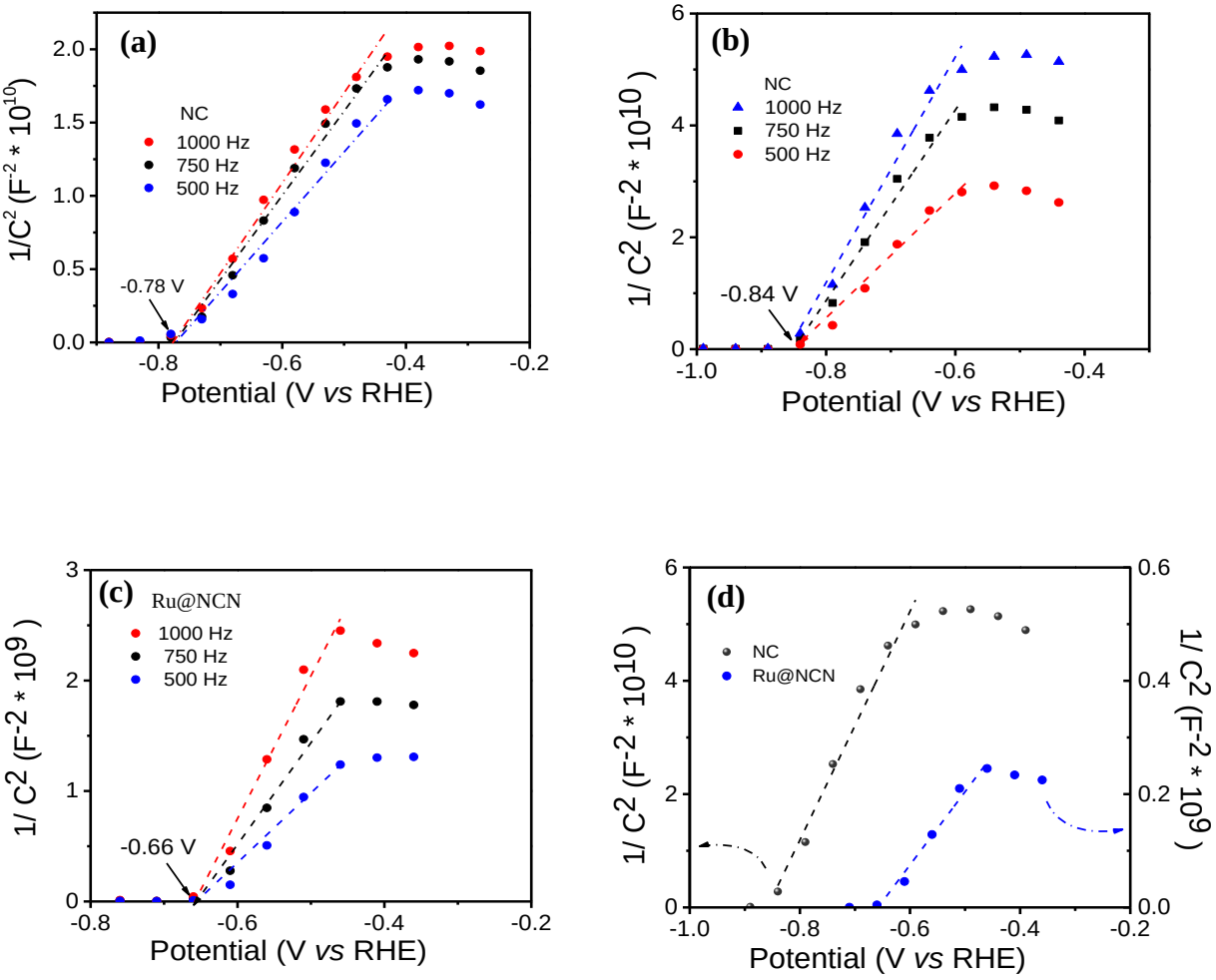

Figure S13. Mott-Schottky plots at different frequencies (1000, 750 and 500 Hz) for NC in (a) acidic media, (b) alkaline media, (c) Ru@NCN in alkaline media and (d) at a fixed frequency of 1000 Hz for NC and Ru@NCN in alkaline media.

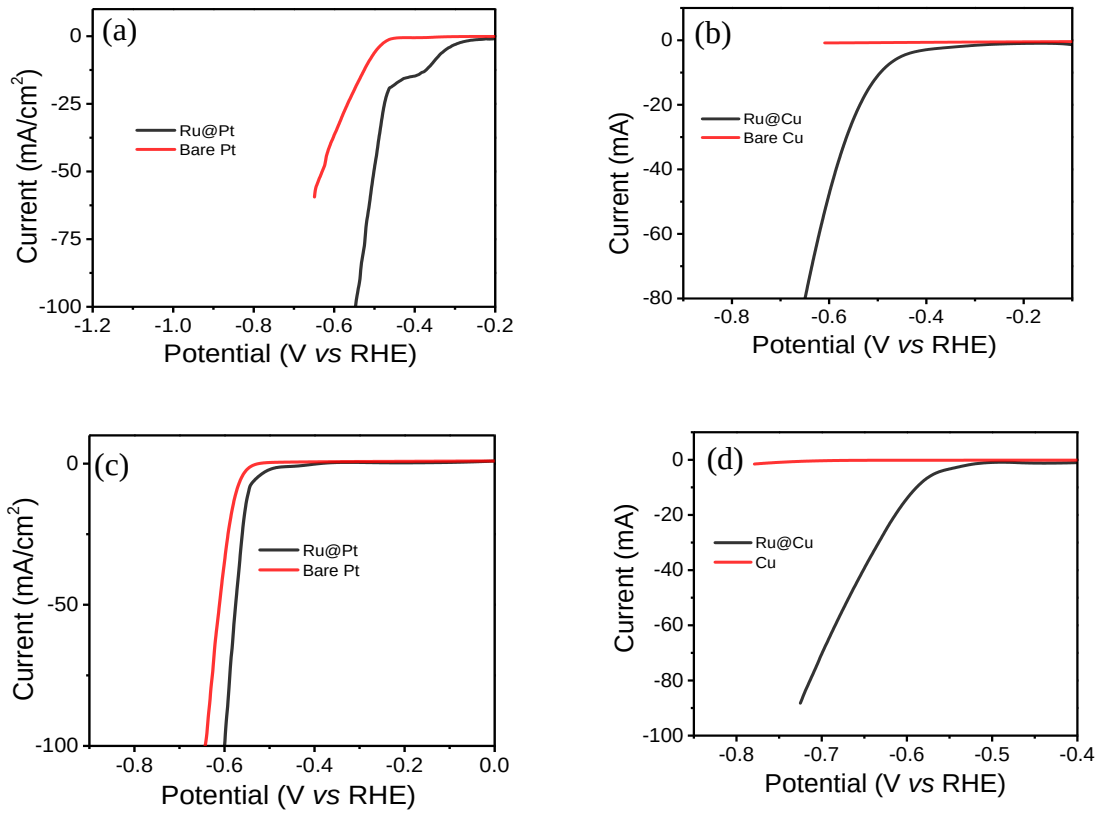

Figure S14. HER LSV polarization curves for the respective samples (Ru@Pt, Pt, Ru@Cu, Cu) in (a, b) 1 M KOH, (c, d) 0.5 M H_2SO_4

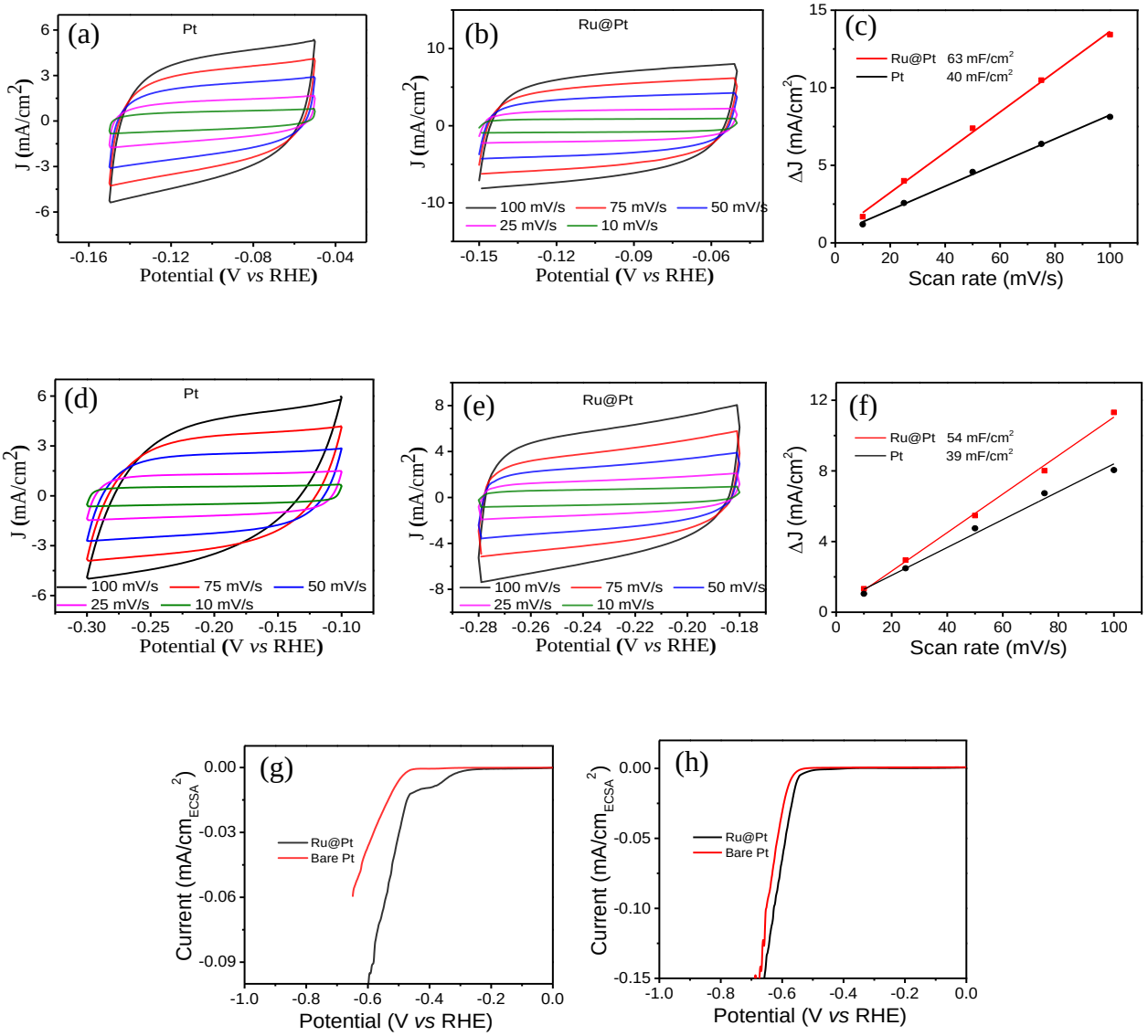

Figure S15. CV in the non-faradaic region at different scan rates (10 to 100 mV/s) to calculate the C_{dl} in (a-c) alkaline, (d-f) acidic media, ECSA normalized LSV polarization curve in (g) alkaline and (h) acidic media for Ru@Pt and bare Pt.

References

1. A. F. Bykov, N. B. Morozova, I. K. Igumenov and S. V. Sysoev, *Journal of thermal analysis*, 1996, **46**, 1551-1565.
2. S. Musić, S. Popović, M. Maljković, K. Furić and A. Gajović, *Journal of Materials Science Letters*, 2002, **21**, 1131-1134.
3. J. B. James and Y. S. Lin, *The Journal of Physical Chemistry C*, 2016, **120**, 14015-14026.
4. D. Wang, Q. Li, C. Han, Z. Xing and X. Yang, *Applied Catalysis B: Environmental*, 2019, **249**, 91-97.
5. Q. Song, X. Qiao, L. Liu, Z. Xue, C. Huang and T. Wang, *Chemical Communications*, 2019, **55**, 965-968.
6. Y. Zheng, Y. Jiao, Y. Zhu, L. H. Li, Y. Han, Y. Chen, M. Jaroniec and S.-Z. Qiao, *Journal of the American Chemical Society*, 2016, **138**, 16174-16181.
7. Z. Pu, I. S. Amiinu, Z. Kou, W. Li and S. Mu, *Angewandte Chemie International Edition*, 2017, **56**, 11559-11564.
8. B. K. Barman, B. Sarkar, P. Ghosh, M. Ghosh, G. Mohan Rao and K. K. Nanda, *ACS Applied Energy Materials*, 2019, **2**, 7330-7339.
9. J. Su, Y. Yang, G. Xia, J. Chen, P. Jiang and Q. Chen, *Nature Communications*, 2017, **8**, 14969.
10. B. K. Barman, D. Das and K. K. Nanda, *Sustainable Energy & Fuels*, 2017, **1**, 1028-1033.
11. J. Wang, Z. Wei, S. Mao, H. Li and Y. Wang, *Energy & Environmental Science*, 2018, **11**, 800-806.
12. B. K. Barman, B. Sarkar and K. K. Nanda, *Chemical Communications*, 2019, **55**, 13928-13931.
13. J. Zhang, P. Liu, G. Wang, P. P. Zhang, X. D. Zhuang, M. W. Chen, I. M. Weidinger and X. L. Feng, *Journal of Materials Chemistry A*, 2017, **5**, 25314-25318.
14. Y. Luo, X. Luo, G. Wu, Z. Li, G. Wang, B. Jiang, Y. Hu, T. Chao, H. Ju, J. Zhu, Z. Zhuang, Y. Wu, X. Hong and Y. Li, *ACS Applied Materials & Interfaces*, 2018, **10**, 34147-34152.
15. T. Qiu, Z. Liang, W. Guo, S. Gao, C. Qu, H. Tabassum, H. Zhang, B. Zhu, R. Zou and Y. Shao-Horn, *Nano Energy*, 2019, **58**, 1-10.
16. H.-S. Park, J. Yang, M. K. Cho, Y. Lee, S. Cho, S.-D. Yim, B.-S. Kim, J. H. Jang and H.-K. Song, *Nano Energy*, 2019, **55**, 49-58.
17. J. Yu, Y. Guo, S. Miao, M. Ni, W. Zhou and Z. Shao, *ACS Applied Materials & Interfaces*, 2018, **10**, 34098-34107.
18. R. G. González-Huerta, J. A. Chávez-Carvayar and O. Solorza-Feria, *Journal of Power Sources*, 2006, **153**, 11-17.
19. H. Teller, O. Krichevski, M. Gur, A. Gedanken and A. Schechter, *ACS Catalysis*, 2015, **5**, 4260-4267.
20. S. Durón, R. Rivera-Noriega, P. Nkeng, G. Poillerat and O. Solorza-Feria, *Journal of Electroanalytical Chemistry*, 2004, **566**, 281-289.
21. C. Zhang, Y. Liu, Y. Chang, Y. Lu, S. Zhao, D. Xu, Z. Dai, M. Han and J. Bao, *ACS Applied Materials & Interfaces*, 2017, **9**, 17326-17336.
22. S. Yuan, Z. Pu, H. Zhou, J. Yu, I. S. Amiinu, J. Zhu, Q. Liang, J. Yang, D. He, Z. Hu, G. Van Tendeloo and S. Mu, *Nano Energy*, 2019, **59**, 472-480.
23. S. Drouet, J. Creus, V. Collière, C. Amiens, J. García-Antón, X. Sala and K. Philippot, *Chemical Communications*, 2017, **53**, 11713-11716.
24. T. Bhowmik, M. K. Kundu and S. Barman, *ACS Applied Materials & Interfaces*, 2016, **8**, 28678-28688.